Experimental Investigation of the Forces Acting on a Drop of Weld Metal

The mass of weld metal droplets during globular transfer is measured as a function of electric current and gas flow

BY J. H. WASZINK AND L. H. J. GRAAT

ABSTRACT. Experiments were carried out in a welding arc having a consumable wire as the positive electrode. The drop mass was measured as a function of the gas flow rate and the electric current. The electrode was surrounded by a hot plasma, so that measurements at zero electrode current could also be made. The various forces acting on a drop at the point of detachment were derived from the measured data.

The following forces were considered: gravity force, the drag force exerted by the flowing gas, electromagnetic force, and the retaining force by the surface tension. The model which was used in the derivation of these forces is based on older work on drop transfer from capillary tubes. The Lorentz force due to the divergence of the electric current within the drop accounts for the electromagnetic force as derived from the measured data.

Introduction

The flow of heat and mass from a consumable electrode to the weld pool governs for a large part the quality of the weld, and the speed of the welding process. The corresponding flow rates are described by the melting rate and the temperature of the transferred liquid metal (Ref. 1-4). Another area of interest is the frequency of drop transfer or, alternatively, the drop mass. Its importance lies in the fact that irregularities in drop transfer lead to irregularities in the weld. Moreover, the momentum of the drops which enter the weld pool affects the depth of penetration (Ref. 5-7). Therefore, it is of interest to investigate how a drop is detached from the wire.

An earlier investigation (Ref. 8) of an overhead welding process showed that drop detachment is influenced by electromagnetic forces. Furthermore, it was found (Ref. 1-9) that the drop mass decreases with increase in the electric current; this also suggests that some electromagnetic effect plays a role. There is a considerable amount of literature dealing with the theory of the mechanism which causes a drop to fall off. A review has been given by Lancaster (Ref. 10). Furthermore, the acceleration of drops after detachment has been measured (Ref. 5, 11).

The literature dealing with the physics of the detachment process can be divided into two main categories according to the basic assumptions made. The model developed by Lancaster (Ref. 12, 13) is based on the assumption that drop detachment is the result of a pinch instability in the liquid wire tip. This model yields the velocity, the acceleration, and the length of a droplet at detachment. A different approach is to assume that a pendent drop becomes unstable and falls off as soon as the downward force on it exceeds the sustaining force due to the surface tension (Ref. 8, 14-16). Although this subject has thus been investigated theoretically, there is, to the authors' knowledge, no direct experimental evidence on the mechanism of drop detachment.

The present paper gives the results of an experimental investigation of the forces which act on a pendent drop, at the moment of detachment (Ref. 17). The mass of the falling drops, M, was measured as a function of the electric current through the electrode, I_w, and the gas flow rate, $\dot{V}$, the electrode being at positive polarity. The measurements were made in a plasma-GMA torch, where the consumable electrode is surrounded by a hot plasma. The apparatus allows drop transfer at zero electrode current, so that the effects of the gas flow and the electric current could be separated easily. The work is limited to globular transfer, i.e., $I_w < 200$ A.

Analysis of the data was based on the assumption that a drop falls off when the detaching force begins to exceed the retaining force. Furthermore, it was assumed that the following forces are acting on the pendent drop:

1. The gravitational force.
2. The drag force exerted by the flowing gas, F_d.
3. A force of electromagnetic origin, F_{em}.
4. The retaining force by the surface tension.

The force exerted by the fluid which enters the drop was not considered. It is of importance at the upper end of the current range only as discussed below. The experiments were carried out with the workpiece in a horizontal plane. The electrode was perpendicular to and above the workpiece (flat welding). The detachment force is then the sum of above forces 1-3.

Treatment of the force due to the surface tension is somewhat different from the treatment given in a previous report (Ref. 17). The difference has only a slight effect on the values of the forces derived.

Experiment

The experiments were carried out with a plasma-GMA torch (Ref. 18) shown schematically in Fig. 1. Here, the arc between the consumable electrode ("wire" in Fig. 1) and the workpiece is surrounded by an outer arc having a carbon ring as its upper electrode. The electrode and the carbon ring were at

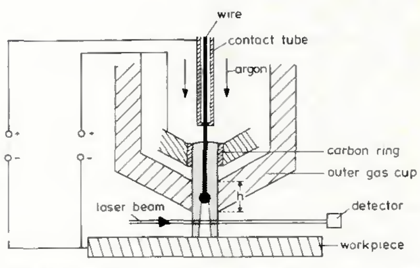

Fig. 1 — Welding torch schematic

J. H. WASZINK and L. H. J. GRAAT are with Philips Research Laboratories, Eindhoven, The Netherlands.

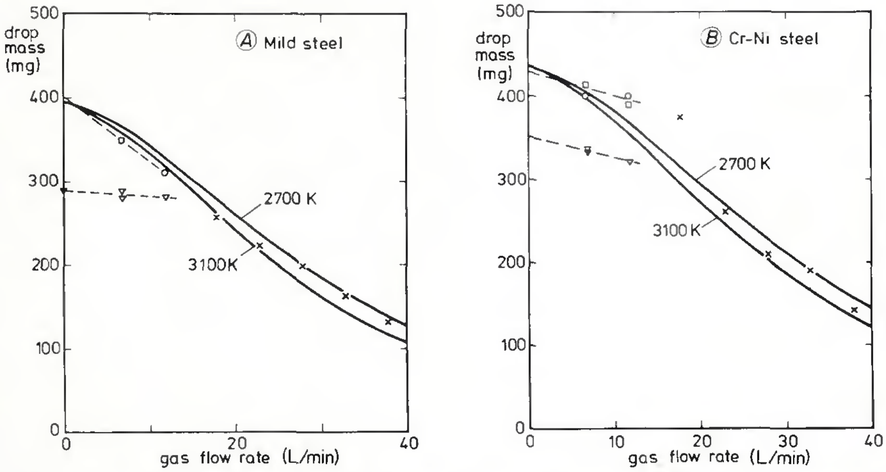

Fig. 2 — Drop mass as a function of gas flow rate at zero electrode current. Gas flow rates measured at room temperature; plasma current — 100 amperes. A — mild steel, calculation for $\gamma = 1.0\ Nm^{-1}$; B — Cr-Ni steel, calculation for $\gamma = 1.1\ Nm^{-1}$. Legend as follows: x — expt., h = 12 mm, $d_w = 1.6$ mm; o — expt., h = 5 mm, $d_w = 1.6$ mm; ∇ — expt., h = 5 mm, $d_w = 1.2$ mm; solid line (_____) — calculation for T_{eff} as indicated (1 in. = 25.4 mm)

positive polarity.

Drop detachment took place in a cylindrical channel in the outer gas cup. The height of this channel, h, was 12 mm (0.47 in.) and its diameter 10 mm (0.39 in.). This arrangement was chosen in order to obtain a well-defined gas flow around the drop. The outer arc was practically cylindrical down to the workpiece, its diameter being equal to the diameter of the channel in the gas cup.

The current through the carbon ring (called the plasma current, I_p) was 100 ± 5 A in all the experiments. The electrode current was varied from 0 to 200 A. The shielding gas was argon. The gas cup described above allowed stable operation at gas flow rates down to 15 L/min (31.8 cfh). Additional measurements at lower flow rates were made with a similar cup, in which h was 5 mm (0.2 in.).

The results of these measurements were used to obtain M for zero gas flow rate. The mass of the falling drops was obtained from the length of wire used in a given time interval, and the number of drops transferred in that time interval. The drops were detected with the aid of a laser beam and a photodetector.

Results

Mild steel and Cr-Ni steel electrodes were used. Their diameter, d_w, was 1.6 mm (0.06 in.). The composition of the electrode material is given in Appendix A. Figure 2 shows M as a function of $\dot{V}$, for $I_w = 0$. Figure 3 shows M as a function of I_w, for different values of $\dot{V}$.

Forces Acting on a Pendent Drop

Relation Between Drop Weight and Detachment Force

Gravitational Force Only. The process of drop detachment from capillary tubes has been investigated extensively (Ref. 19-22). The analysis of the data given in Figs. 2 and 3 is based on this work. Conditions for the detachment of a drop, which is subjected to the gravitational force only, are discussed below.

The mass of a pendent drop, M_p, is given by the relation (Ref. 21):

$$M_p\, g = 2\pi\, R_w \gamma \left\{ \sin\phi - \left(\frac{R_w}{2R_1} + \frac{R_w}{2R_2} \right) \right\} \qquad (1)$$

where g is the gravity constant, γ is the surface tension, R_w is the tube radius, ϕ is the contact angle between a horizontal plane and the surface of the liquid, R_1 and R_2 are the radii of curvature of the surface; and ϕ, R_1, and R_2 are to be taken in the plane where the liquid is in contact with the solid tip. As a drop grows, it reaches a critical mass M_{pc} and becomes unstable. A part of the liquid will then fall off. Calculations by Lohnstein (Ref. 19) showed that the mass of a falling drop, M, can be written as:

$$M\, g = 2\,\pi\, R_w\, \gamma\, f\,(R_w/a) \qquad (2)$$

where a is the capillary constant, a $\equiv (2\gamma/\rho\ g)^{1/2}$, and ρ the mass density. The factor f accounts for the expression between brackets in equation (1), and for the fact that a part of the liquid remains on the tip after detachment. This factor is a function of the ratio R_w/a {$= (R_w^3\ \rho\ g/2\ \gamma\ R_w)^{1/2}$}, which is a measure of the detaching gravitational force and the retaining force by the surface tension. Equation (2) can also be written as:

$$M\, g = 2\,\pi\, R_w \gamma \psi\ (M/\rho\ R_w^3), \qquad (3)$$

where $\psi(M/\rho\ R_w^3)$ is a function equal to f (R_w/a). The function f was calculated by Lohnstein (Ref. 19), and ψ was measured by Harkins and Brown (Ref. 2). Their results are in good agreement for $0 \leq R_w/a \lesssim 2.0$ (Ref. 21).

Both f and ψ are available in tabulated form. Equation (3) allows direct calculation of γ from the measured drop weight.

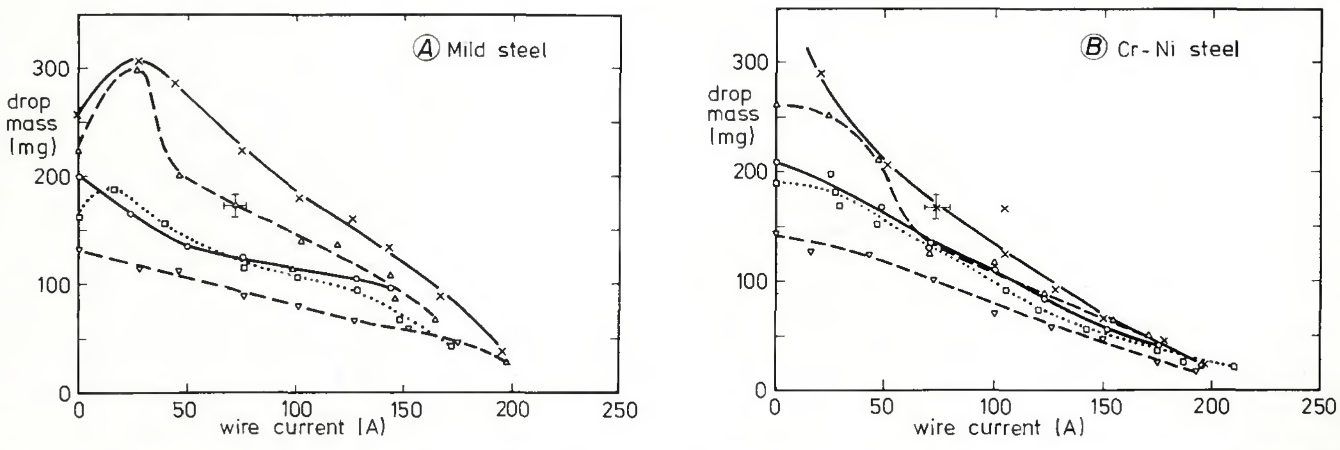

Fig. 3 — Measured drop mass: A — mild steel; B — Cr-Ni steel. $d_w = 1.6$ mm; x — $\dot{V} = 18$ L/min, △ — $\dot{V} = 23$, o — $\dot{V} = 28$; □ — $\dot{V} = 33$, ∇ — $\dot{V} = 38$ (1 in. = 25.4 mm)

Experiments by Calverley (Ref. 23) showed that equation (3) is also applicable if drops are detached from a melting wire. The tube radius must then be replaced by the wire radius, and R_w now denotes the latter quantity.

Force Not Purely Gravitational. The detachment force of a drop of weld metal is the sum of the force due to gravity, the force due to drag by the gas, and a force due to electromagnetic effects. Consequently, the force per unit volume is larger than in the purely gravitational force field.

Equations (1) to (3) can be retained formally if R_w/a is replaced by a larger effective value, $(R_w/a)_{eff}$. The smallest drop size measured in the experiments described here was about 30 mg. It then follows from equation (2) and a table of f (R_w/a) values that $(R_w/a)_{eff}$ is 0.5 or less.

The results obtained by Hartland and Srinivasan (Ref. 21) show that $\sin \phi$ is then the major term between the brackets in equation (1), and that $\sin \phi \approx 1$. Their work is only a rough guide to the process of drop detachment in welding, because the shape of the drop surface depends on the spatial distribution of the force field within the drop.

As an approximation it is assumed that $\sin \phi = 1$; the curvature terms in equation (1) are neglected, thus giving:

$$2 \pi R_w \gamma \approx M_{pc} + F_d + F_{em} \quad (4)$$

and,

$$M = M_{pc} \psi (M/\rho R_w^3). \quad (5)$$

Furthermore, a table of ψ (Ref. 24) for a purely gravitational force was used.

The Drag Force

The force exerted on a spherical body in a flowing gas, in the direction of the flow, can be written as (Ref. 25):

$$F_d = C_d \frac{\rho v^2}{2} \pi R^2 \quad (6)$$

where v is the flow velocity, R the radius of the sphere, and C_d the drag coefficient; the latter quantity is a function of the Reynolds number, $Re = 2 R \rho v/\eta$, where η is the viscosity.

The relation between C_d and Re is well established for spherical bodies. A pendent drop is, however, partly screened by the electrode. As an approximation, we have used the values of C_d for a sphere, C_{ds} (Ref. 25), multiplied by a factor $1 - R_w^2/2 R^2$, where R is the drop radius. This correction was also used by Needham, et al. (Ref. 11) and is discussed in their paper. The expression for F_d thus becomes:

$$F_d = C_{ds} (1 - R_w^2/2 R^2) \frac{\rho v^2}{2} \pi R^2 \quad (7)$$

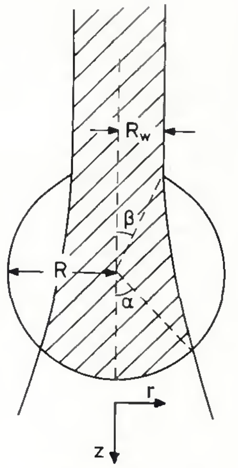

Fig. 4 — Illustration for discussion of $\vec{j} \times \vec{B}$ force

The Electromagnetic Force.

The diameter of the anode spot, where the current leaves the drop, is in general not equal to the electrode diameter. Consequently, the current diverges or converges within the drop and a force $\vec{f_L} \equiv \vec{j} \times \vec{B}$ (the Lorentz force), is exerted on a unit volume of liquid metal (Ref. 8, 14, 16); $\vec{j}$ is the current density, and $\vec{B}$ the magnetic induction. Its radial and axial components in cylindrical (r, Θ, z) coordinates (Fig. 4) are:

$$(f_L)_r = - j_z B_\Theta \quad (8)$$

$$(f_L)_z = + j_r B_\Theta \quad (9)$$

where cylindrical symmetry has been assumed.

The force on a drop, F_L, is the integral of $(f_L)_z$ over the drop volume. For a spherical drop, and a spatially homogeneous distribution of j_z it is given by (Ref. 14, 16):

$$F_L = \frac{\mu_0 I_w^2}{4 \pi} \chi (\alpha, \beta) \quad (10)$$

where

$$\chi (\alpha, \beta) = \ln \left(\frac{\sin \alpha}{\sin \beta}\right) - \frac{1}{4} + \frac{1}{1 - \cos \alpha} + \frac{2}{(1 - \cos \alpha)^2} \ln \left(\frac{2}{1 + \cos \alpha}\right) \quad (11)$$

μ_0 is the permeability of vacuum, and the angles α and β are given in Fig. 4. The electromagnetic force induced by fluid flow is negligible, because the parameter $K \equiv \mu_0^{3/2} \sigma I_w/\rho^{1/2}$, introduced by Shercliff (Ref. 26) is small, $K \approx 10^{-3}$ (σ is the electrical conductivity of the liquid metal).

A Lorentz force will also be exerted on the plasma, causing an increase in pressure and thus an upward force on the drop. This point will be discussed below.

Physical Properties of the Arc-Electrode System

There are two points which require examination:

1. An estimate must be made of the static pressure below the drop.
2. The relation between the measured wire current, I_w, and the current through the drop must be established; these currents are not necessarily equal, because electrons may enter the electrode above the drop.

The plasma below the electrode tip is divided into two regions having different physical properties (Ref. 27, 28). First, there is a narrow cylinder around the axis, whose diameter is about 2 mm (0.08 in.) where the plasma contains metal vapor (Fe, Mn). The temperature, T, is about 7000 K (7000°C, 12000°F) there, and the electron density, n_e, about 10^{22} m^{-3} (Ref. 27). The outer region of the plasma contains argon only, and both T and n_e are much higher (13000 K $\approx$ 13000°C $\approx$ 23000°F and 10^{23} m^{-3}, respectively — Ref. 27).

Pressure in the Plasma Below the Drop

The electrode and plasma currents, I_w and I_p respectively, are of comparable magnitude. Therefore, the current density will be much higher within the electrode (≈ 75 A/mm^2) than in the surrounding plasma (≈ 1 A/mm^2). This will still be so at the surface of the electrode tip where the electrode current enters the plasma.

On the other hand, it was shown by Ton (Ref. 27) that the colder metal plasma carries only a small part of the total arc current. It then follows that the current I_w must diverge strongly after entering the plasma. Consequently, the arc current in the plasma below the wire tip is the sum of the current I_p which has a broad spatial distribution, independent of the vertical coordinate, and a diverging current I_w. The corresponding current densities will be denoted by j_p and j_w, respectively.

The Lorentz force, as given by equations (8) and (9), also acts on the plasma, and its radial component causes an increase in pressure at the axis. If the plasma were stationary, then this excess pressure would be proportional to the product $I (j_w + j_p)$, and it would practically compensate the downward electromagnetic force on the drop. Since, however, j_w decreases with increase in z (coordinates as in Fig. 4), it follows that the excess pressure decreases with increase in z. As a result, there will be a gas flow (Ref. 29) which reduces the static pressure.

An estimate given in Appendix B indicates that this pressure will be small when the flow velocity is about 100 m/s. Experiments by Wienecke (Ref. 30) yielded velocities of this order of magnitude. Therefore, we may neglect the static pressure.

Current Drawn by the Electrode

The lower half of the electrode is in contact with the argon plasma (Fig. 1), except for the tip which is in contact with the colder metal plasma. Each part of the electrode surface will draw a current from the plasma, whose direction and magnitude depend on the local difference between the electrode potential V_w, and the plasma potential V_p.

There is extensive literature on electrical probes in plasma (Ref. 31). However, to the authors' knowledge, there is no treatment available which directly yields the current density at the electrode surface as a function of the vertical distance along the wire.

Appendix C gives an approximate treatment which is based on the physical model developed by Waymouth (Ref. 32) for a spherical probe. This treatment leads to the following results:

1. The difference $\Delta V \equiv V_w - V_p$ is close to zero at the anode spot on the drop.
2. There is a potential difference between the metal vapor plasma in the center, below the wire tip, and the surrounding arc plasma, the latter having the higher potential. This difference is caused by ambipolar diffusion of ions and electrons from the outer plasma, where $n_e \approx 10^{23}$ m^{-3}, to the inner plasma, where $n_e \approx 10^{22}$ m^{-3}.
3. Both V_p and V_w increase in the direction upwards from the wire tip, the increase in V_p being faster.

The sum of these contributions reveals that ΔV becomes negative along the whole length of the electrode. The electron current which enters the electrode above the drop is estimated to be about 5 A. It is partly compensated by the ion current (about 4 A) which enters in the upper part of the wire. Consequently, the current which bypasses the drop is small, and it will be assumed in the analysis given below that the current through the drop is equal to I_w.

Analysis of Experimental Data

This section deals with the derivation of the forces F_d and F_{em} from the experimental data with equations (4), (5) and (7). The procedure is to determine γ from data for $F_d = 0$ ($\dot{V} = 0$) and $F_{em} = 0$ ($I_w = 0$). Next, the force F_d is obtained from experiments with $\dot{V} \neq 0$, and $I_w = 0$. Finally, the force F_{em} is obtained from the experiments with $\dot{V} \neq 0$, $I_w \neq 0$.

The drop mass for zero gas flow and zero wire current was determined by extrapolation of the curve of M vs $\dot{V}$, obtained with the shorter nozzle—Fig. 2. Equations (4) and (5) then yield γ. It was found that $\gamma = 1.0 \pm 0.05$ Nm^{-1} for the mild steel, and $\gamma = 1.1 \pm 0.05$ Nm^{-1} for the Cr-Ni steel. The main constituents of the wire material are Fe, Cr, Ni, and Mn. The surface tensions of the pure liquid metals at their melting points are 1.83, 1.70, 1.75, and 1.10, respectively (Ref. 33). The results thus suggest that Mn is the dominant constituent at the drop surface.

In discussing experiments conducted with nonzero gas flow and zero electrode current, the first question is whether F_d can be represented by equation (7). Furthermore, the quantities ρ and η, which depend on the temperature, must be determined. There is, however, a steep temperature gradient in the boundary layer around the electrode, so that an effective temperature T_{eff} will be used. The relation between v and $\dot{V}$ follows from the equality of the masses passing through the flow meter and the channel in the outer gas cup:

$$S\, v\, \rho\, (T_{eff}) = \dot{V}\, \rho\, (T_0) \qquad (12)$$

where S is the cross sectional area of the channel, and T_0 the temperature at which $\dot{V}$ was measured (295 K = 22°C = 72°F).

The parameters η (Ref. 34) and ρ are to be taken at T_{eff}. The drop radius, R, was determined on the assumption that the drop is a truncated sphere, so that M and R are related by:

$$M = \rho_m \left\{\frac{4}{3}\pi R^3 - \frac{1}{6}\pi X (3 R_w^2 + x^2)\right\}, \qquad (13)$$

$$\text{where } x \equiv R - (R^2 - R_w^2)^{1/2}. \qquad (14)$$

Equations (4), (5), (7), (12)—(14), and the relationship between C_{ds} and Re now yield M as a function of $\dot{V}$, for $F_{em} = 0$, and with T_{eff} as a parameter. The density ρ was taken to be 7000 kg · m^{-3}, i.e., the value at the melting point. The resulting curve for M vs. $\dot{V}$ was fitted to the experimental curves, by adjustment of T_{eff}.

Figure 2 shows that a good fit is obtained. The corresponding value of T_{eff} is 2900 ± 200 K (2600°C, 4700°F, $\eta = 1.18 \times 10^{-4}$ kg · m^{-1} s^{-1}, $\rho = 0.17$ kg · m^{-3}). This temperature is well below the plasma temperature, as determined spectroscopically (Ref. 27). The cause of this difference is most likely that v and the gas temperature are not independent of the radial position as was implied by the use of the drag coefficient.

Both the thermal and the velocity boundary layer (Ref. 35) are rather thick (1-2 mm, i.e., 0.04-0.08 in.), and the value obtained for T_{eff} suggests that the drag on the drop is determined by the flow speed in this layer. On the other hand, the good agreement between the calculated and the measured curves of M vs. $\dot{V}$ indicates that equation (7) gives an adequate description of the drag force on the drop. The values obtained for F_d are applicable only to the arc system discussed here. This is because the diameter of the nozzle channel and the gas temperature inside it determine the relation between v and $\dot{V}$.

It is to be noted that F_d will be lower in a GMA system than in a plasma-GMA system, as was used here. The difference is due to the fact that the gas which impinges on the drop is practically at room temperature in a GMA process, while it is around 10000 K (≈ 10000°C ≈ 18000°F) in a plasma-GMA process. Consequently, the gas velocity and the drag force will be higher in the latter system.

Finally, the electromagnetic force was derived from the data for nonzero electrode current. There are a few points which require discussion concerning the analysis of these data:

1. The bulk temperature of the drop will be higher when $I_w \neq 0$ than when $I_w = 0$. In the arc discussed here ($I_w \neq 0$) it is about 2400 K (≈ 2100°C ≈ 3800°F, Ref. 2 and 3). The density ρ was taken at this temperature ($\rho = 6500$ kg m^{-3}) for the results for $I_w \neq 0$.
2. The surface tension decreases with increase in temperature, so that γ will now be lower than at zero electrode current. The temperature distribution along the drop surface was measured by Villeminot (Ref. 36) in a gas metal arc. His measurements show that the temperature at the upper end of the drop, which is the relevant region in this analysis, lies between the melting point, T_m, and T_m + 1000 K. As an average, we take γ at T_m + 500 K, with an uncertainty of 250 K. Since $d\gamma/dT \approx -0.2 \times 10^3$ N m^{-1} K^{-1} for Mn (Ref. 37), $\gamma = 0.90 \pm 0.05$ N m^{-1} for the mild steel, and $\gamma = 1.00 \pm 0.05$ for the Cr-Ni steel.
3. The plasma which surrounds the electrode, tends to contract when I_w increases, as observed previously. This effect may change the flow pattern around the electrode. A simple estimate based on equation (8), with v = 0 at the electrode surface, reveals that the increase in pressure at this surface is about 10^{-3} atm for an increase of 200 A in I_w. Consequently, this effect is small and will be neglected.
4. The surface tension changes if there is a surface charge, q. According to (Ref. 38) $|q| = |\partial\gamma|\partial V|$, where V is the difference in potential between drop and plasma. The drop will carry some surface charge, because it is surrounded by a space charge layer (Appendix C). The thickness of this layer is about 1 μm and the potential difference about 6 V when the tip is at the floating potential ($I_w = 0$). The drop surface and the edge of the space charge layer can be considered as a spherical capacitor, and it follows that the resulting error in γ is of the order of

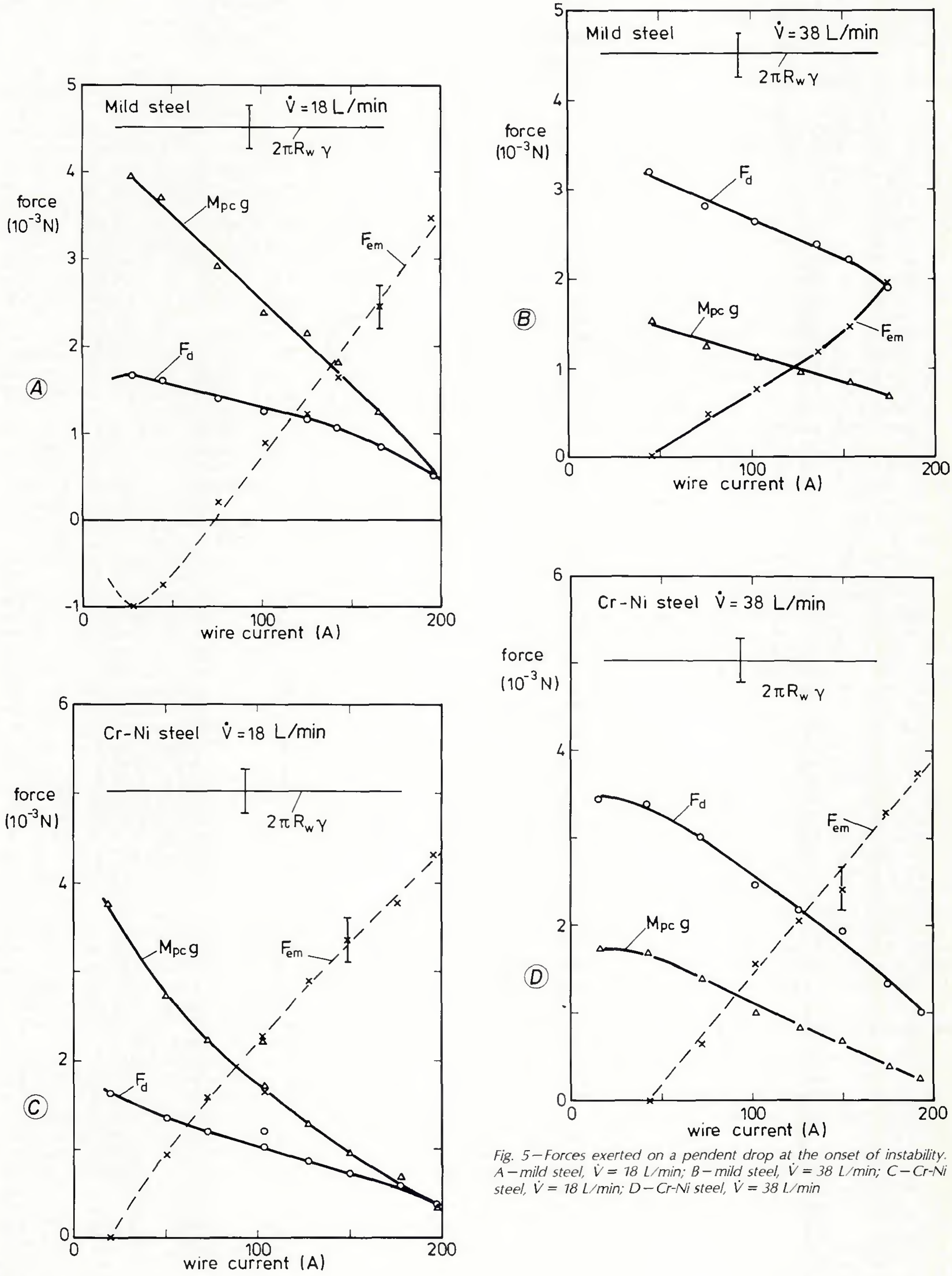

Fig. 5—Forces exerted on a pendent drop at the onset of instability. A—mild steel, $\dot{V}$ = 18 L/min; B—mild steel, $\dot{V}$ = 38 L/min; C—Cr-Ni steel, $\dot{V}$ = 18 L/min; D—Cr-Ni steel, $\dot{V}$ = 38 L/min

10^{-3} N m^{-1}, i.e., well within the error limit given above.

The force F_{em} was derived with equations (4), (5), (7), (12)-(14), i.e., by subtraction of the gravitational and drag forces from the surface tension force. Consequently, the relative error is large when F_{em} is small, the main source of error being the uncertainty in γ.

Figures 5A and 5D show the forces which act on a drop. A negative value of F_{em} indicates an upward force. The radii R lie between 1.0 and 2.5 mm (0.04 and 0.1 in.), and v as obtained from equation (12) between 40 and 80 m/s. Figures 5A and 5B show that F_{em} increases, in general, with increase in I_w, except for mild steel at low currents, where it becomes negative.

Analysis of the Electromagnetic Force

Results With Mild Steel. It now has to be verified whether F_{em}, as derived above, can be interpreted as the Lorentz force, as given by equations (10) and (11). Calculation of F_L from these equations requires knowledge of the angles α and β—Fig. 4.

Both angles increase with an increase in I_w, because R then decreases and the diameter of the anode spot increases. The drop radius follows from M, and it was found that sin β ($=R_w/R$) lies between 0.3 and 0.8. The angle α cannot be derived from the experiment. The function χ from equation (11) is negative for small α. It increases with increase in α, becomes zero when $\alpha \approx \beta$, and reaches a maximum just above $\alpha = \pi/2$.

The maximum value of χ is 1.4 for sin $\beta = 0.3$, and 0.5 for sin $\beta = 0.8$. A negative, i.e., an upward force, will occur when $\alpha < \beta$. Normally, $\alpha > \beta$, so that χ and F_L are positive. Values of χ between 0.2 and 1.4 are thus expected. This is, in fact, found for mild steel at electrode currents above 100 A—Fig. 6. The results for mild steel yield negative values of F_{em} at the lower currents for $\dot{V}$ = 18 (Fig. 6A), 23, and 33 L/min (38, 48.7, and 69.9 cfh).

These values are rather inaccurate as previously indicated. However, it is certain that they are negative, because the raw data (Fig. 3A) show an initial increase in M with increase in I_w.

It follows from equations (10) and (11) and the discussion given above that an upward force, if it occurs at all, will occur when the anode spot is small, i.e., when I_w is low. The hypothesis that F_{em} is the Lorentz force thus accounts for the upward force, and for the fact that it is found at low currents only. The value of F_L cannot be calculated directly from equations (10) and (11), because α is not known. Therefore, the assumption was made that the current density in the anode spot, j_A, has a given constant value, independent of I_w. The angle α is then given by:

$$\cos \alpha = 1 - \frac{I_w}{2\,\pi\,R^2\,j_A}, \qquad (15)$$

so that F_L can be calculated from R and I_w, and an assumed value of j_A.

Figure 6 shows that the curve obtained for j_A = 15 A/mm² is in reasonable agreement with the experimental data, except for the upper and lower ends of the current range. The negative points at low I_w indicate a very high current density. At currents close to 200 A, the model as used here ceases to be valid. The drop is then formed at the pointed electrode tip (Ref. 39), and the radius of the drop neck is no longer equal to the electrode radius. Moreover, a part of the electrode current bypasses the drop and accelerates the liquid metal which flows down the pointed tip of the solid electrode.

The liquid entering the drop exerts an appreciable force on the droplet. As the current is increased, the kinetic pressure of the incoming liquid becomes so high that drop formation is impossible, and a jet (spray transfer) is formed (Ref. 4). Consequently, the Lorentz force remains operative, but its formulation as given by equations (10) and (11) is not applicable when I_w is close to 200 A.

Lancaster (Ref. 40) used equations (10) and (11) to calculate F_L from the size of the drop and the current-carrying area as reported by Pintard (Ref. 39, mild steel, R_w = 0.06 mm, GMA, argon). Figure 6A shows these points which lie close to the points for F_{em}.

Results With Cr-Ni Steel. Figure 7 shows the data obtained with Cr-Ni steel, and $\dot{V}$ = 28 L/min (59.3 cfh). This curve lies close to the curves for the other gas flow rates. It is seen that F_{em} is positive everywhere, and that it lies well above the curve of $\mu_0 I_w^2/4\pi$ vs. I_w (cf. equation (10)). The experimental points cannot be represented by equations (10), (11), and (15), and an assumed valve of j_A. On the other hand, the experimental points lie close to the curve of $\mu_0 I_w^2/4\pi$ vs. I_w; this suggests that F_{em} is the Lorentz force.

There is a possible explanation for the discrepancy:

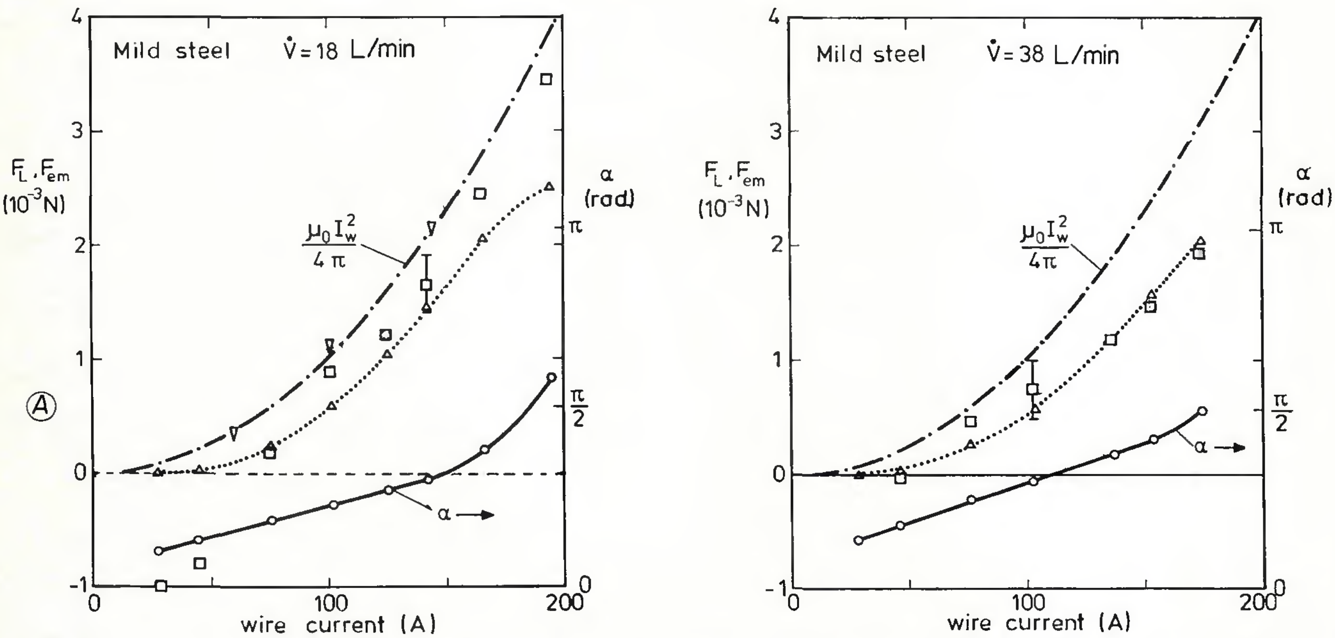

Fig. 6—Comparison of electromagnetic force, as derived from experimentation, with calculated Lorentz force—mild steel: A—$\dot{V}$ = 18 L/min; B—$\dot{V}$ = 38 L/min. □—F_{em}, ...Δ. . . .F_L calculated from equations (10), (11) and (15) and experimental value of R, with $j_A = 1.5 \times 10^7$ A m^{-2}. ∇—F_L calculated by Lancaster. ___ . ___ equation (10) with $\chi = 1.0$. o—α as derived from equation (15) and R, with j_A as above

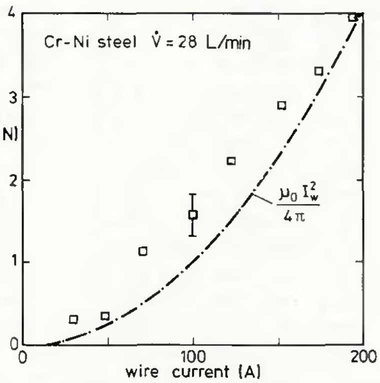

Fig. 7—Electromagnetic force derived from measured data for Cr-Ni steel

1. γ might be lower than was assumed.

2. The discrepancy might be due to assumptions made in the model, in particular the omission of the curvature terms from equation (1), the neglect of gradients in γ, or the assumption of a homogeneous current density.

Summarizing this section, the electromagnetic force derived from the experimental data for mild steel is in good agreement with the Lorentz force as given above. The occurrence of negative values, in particular, supports the hypothesis that F_{em} is the Lorentz force resulting from the divergence of the current within the drop. The slope of the curves obtained for Cr-Ni steel appears to agree with the model, but the values of the force are too high, roughly by a factor 2. On the other hand, realizing that the model used in the analysis is approximate, the agreement is considered to be reasonable.

Substituting F_L (equation (10)) for F_{em}, and equation (7) for F_d into equation (4), yields the relation for M as a function of I_w, $\dot{V}$, and R_w.

The set of equations is completed by equations (5) and (11)-(14). This holds for a given process (GMA, plasma-GMA) and torch geometry, and given electrode material and shielding gas. The set of equations cannot be solved analytically, but the numerical solution is simple.

Conclusion

The drop mass was measured as a function of the electric current through the electrode and the gas flow rate. The electrode was at positive polarity, and the drop transfer was globular. The use of a plasma-GMA torch allowed experiments at zero electrode current.

The drag force exerted by the imposed gas flow, and a force of electromagnetic origin were derived from the measured data. Calculated values of the Lorentz force are in good agreement with values of the electromagnetic force derived from the data for mild steel, while the data for Cr-Ni steel give a reasonable agreement.

Some of the experiments yielded an upward electromagnetic force, further confirming the interpretation of the electromagnetic force as the Lorentz force.

Acknowledgments

The authors are indebted to J.F. Lancaster and G.W. Tichelaar for helpful comments.

References

1. Lesnewich, A., 1958. Control of melting rate and metal transfer in gas shielded metal arc welding. *Welding Journal* 37 (8): 343-s to 353-s, and 37 (9), 418-s to 425-s.

2. Jelmorini, G., Tichelaar, G.W., and Van den Heuvel, G.J.P.M. 1977. *Droplet temperature measurements in arc welding.* IIW-doc. 212-411-77.

3. Van den Heuvel, G. J. P. M., Jelmorini, G., and Tichelaar, G. W. 1978. Messung der Tropfentemperatur im Schweisslichtbogen und Ihre Bedeutung in der Praxis. *DVS Ber.* 50:165-171.

4. Waszink, J. H. and Van den Heuvel, G. J. P. M. 1982. Heat Generation and Heat Flow in the Filler Metal in GMA Welding. *Welding Journal* 61(8):269-s to 282-s.

5. Pintard, J. 1967. Caractéristiques de la fusion et du transfert dans le procédé MIG de soudage de l'acier sous argon. *Soudage et Techniques Connexes* 21:381-393.

6. Essers, W. G., and Walter, R. 1979. Some aspects of the penetration mechanisms in metal-inert-gas (MIG) Welding. *Proc. Int. Conf. on Arc Physics and Weld Pool Behaviour*, pp. 289-300. Cambridge, England: The Welding Institute.

7. Essers, W. G., and Walter, R. 1981. Heat Transfer and Penetration Mechanisms with GMA and Plasma-GMA Welding. *Welding Journal* 60 (2): 37-s to 42-s.

8. Sack, J. 1939. Overhead welding. *Philips Techn. Rev.* IV: 9-15.

9. Cooksey, C. J. and Milner, D. R. 1962. Metal Transfer in Gas-Shielded Arc Welding. *Proc. Symposium Physics of the Welding Arc*, pp. 123-132. Cambridge, England. The Welding Institute.

10. Lancaster, J. F. 1979. Metal transfer in fusion welding. *Proc. Int. Conf. on Arc Physics and Weld Pool Behaviour*, pp. 135-146. Cambridge, England: The Welding Institute.

11. Needham, J. C., Cooksey, C. J., and Milner, D. R. 1960. Metal Transfer in Inert-Gas Shielded-Arc Welding. *Brit. Weld. J.* 7: 101-114.

12. Lancaster, J. F. 1978. *Mass flow in fusion welding.* IIW doc. 212—429—78.

13. Lancaster, J. F. 1980. *Metallurgy of Welding*, Chap. 3. London: Allen and Unwin.

14. Greene, W. J. 1960. An Analysis of Transfer in Gas-Shielded Welding Arcs. *AIEE Trans., part II: Applications and Industry* 79: 194-203.

15. Amson, J. C., and Salter, G. R. 1962. An Analysis of the Gas-Shielded Consumable-Metal Arc Welding System. *Proc. Symposium "Physics of the Welding Arc,"* pp. 133-147. Cambridge, England: The Welding Institute.

16. Amson, J. C. 1965. Lorentz force in the molten tip of an arc electrode. *Brit. J. Appl. Phys.* 16: 1169-1179.

17. A short version of this report, entitled "Der Einfluss der Gasströmung auf die Tropfenablösung beim Plasma-MIG Schweissen" was presented at the "Grosse Schweisstechnische Tagung" of the DVS, October 1979, DVS Berichte 57, 1979, pp. 198-203.

18. Essers, W. G., Tichelaar, G. W., and Williams, G.A.M. 1977. Plasma-MIG-Schweissen von Aluminium. *Aluminium* 53 (11): 663-666; see also IIW doc. IV-242-78.

19. Lohnstein, Th. 1906. "Zur Theorie des Abtropfens mit besonderer Rücksicht auf die Bestimmung der Kapillaritäts-konstanten durch Tropfversuche. *Ann. Physik* 20: 237-268.

20. Harkins, W. D., and Brown, F. E. 1919. The determination of surface tension (free surface energy), and the weight of falling drops: the surface tension of water and benzene by the capillary height method. *J. Am. Chem. Soc.* 41: 499-524.

21. Hartland, S., and Srinivasan, P. S. 1974. The Basis of Theoretical Correction Factors for Use with the Drop Weight Method of Surface Tension Measurement. *J. Colloid and Interface Science* 49(2): 318-320.

22. Boucher, E. A., and Evans, M. J. B. 1975. Pendent drop profiles and related capillary phenomena. *Proc. Roy Soc. Lond.* A 346, 349-374.

23. Calverley, A. 1957. A Determination of the Surface Tension of Liquid Tungsten by the Drop-Weight Method. *Proc. Phys. Soc.* B 70, 1040-1044.

24. Adam, N. K. 1930. *The Physics and Chemistry of Surfaces*, 312 ff. Oxford: Clarendon Press.

25. Schlichting, H. 1968. *Boundary-Layer Theory*, 6th Ed., Chap. I. New York McGraw-Hill.

26. Shercliff, J. A. 1970. Fluid motions due to an electric current source. *J. Fluid Mech.* 40(2): 241-250.

27. Ton, H. 1975. Physical properties of the plasma-MIG welding arc. *J. Phys. D: Appl. Phys.* 8: 922-933.

28. Essers, G. W., Jelmorini, G., and Richelaar, G. W. 1972. Electrode phenomena with plasma-MIG welding. *Proc. 2nd Int. Conf. on Gas Discharges*, pp. 135-137. London: IEE.

29. Maecker, H. 1955. Plasmaströmungen in Lichtbögen infolge eigenmagnetischer Kompression. *Z. Physik* 141:198-216.

30. Wienecke, R. 1955. Ueber das Geschwindigkeitsfeld der Hochstromkohlebogensäule. *Z. Physik* 143:128-140.

31. Swift, J. D., and Schwar, M. J. R. 1970. *Electrical Probes for Plasma Diagnostics*, Chap. 10. London: Iliffe Books.

32. Waymouth, J. F. 1964. Perturbation of a Plasma by a Probe. *Phys. Fluids* 7(11):1843-1854.

33. Lang, G. 1976. Abschatzung unbekanntter Oberflächen-spannungswerte von flüssigen Metallen. *Z. Metallkunde* 67(8):549-558.

34. Amdur, I., and Mason, E. A. 1958. Properties of Gases at Very High Temperatures. *Phys. Fluids* 1(5):370-383.

35. For the relevant relations see e.g., Tritton, D. J. 1977. *Physical Fluid Dynamics.* New York: Van Nostrand Reinhold.

36. Villeminot, P. 1967. Soudage MIG sous argon d'acier doux, étude thermique de la partie terminale, température de transfert. *Soudage et Technique Connexes* 21(9/10): 367-380.

37. Lang, G. 1977. Kritische Temperaturen und Temperatur-koeffizienten der Oberflächenspannung flüssiger Metalle. *Z. Metallkunde* 68(3):213-218.

38. See e.g., J. J. Bikerman, 1958. *Surface Chemistry*, Chap. VI. New York: Academic Press.

39. Pintard, J. 1966. *Formation et croissance*

des gouttes. Forces auxquelles elles sont sur-mises avant et pendant le transfert. IIW Doc. 212-89-66.

40. Lancaster, J. F. 1979. private communication.

41. Dinulescu, H. A., and Pfender, E. 1980. Analysis of the anode boundary layer of high intensity arcs, *J. Appl. Phys.* 51(6):3149-3157.

42. Griem, H. R. 1964. *Plasma Spectroscopy,* Chap. 6. New York: McGraw-Hill.

43. Delcroix, J. L. 1966. *Physique des Plasmas,* vol. 2, Chap. 16. Paris: Dunod.

44. Edmonds, T. G., Allum, C. J., Pinfold, B. E., and Nixon, J. H. 1979. The effects of pressure on the tungsten argon welding arc. *Proc. Int. Conf. on Arc Physics and Weld Pool Behaviour,* pp. 101-107. London, Cambridge, England: The Welding Institute.

Appendix

A. Electrode Compositions

The following compositions were provided by the manufacturer:

Mild steel. 0.06–0.12% C; 1.30–1.70% Mn; 0.70–0.95% Si; 0.01% max. Al.

Cr-Ni steel. 0.03% max. C; 1.8% Mn; 0.85% Si; 20.5% Cr; 9.5% Ni.

B. Pressure in the Plasma Below the Electrode Tip

It is assumed that there is a flowing, homogeneous, cylindrical plasma (current density j_p, velocity v_1, pressure p_1) with, at its axis, a current carrying wire electrode, and, below the electrode, a conical region which carries an excess current I_w (current density j_w). This excess current causes an increase in the plasma pressure just below the electrode tip.

It is shown below that this increase in pressure is small, so that the resulting upward force on the drop is negligible:

The flowing gas is assumed to be stationary ($\partial/\partial t = 0$) and inviscid. The Navier-Stokes equation then reads:

$$\rho(\vec{v} \cdot \vec{\nabla})\vec{v} = -\vec{\nabla} p + \vec{f_L} \qquad (B1)$$

where $\vec{v}$ is the gas velocity, and p the static pressure. Integration of equation (B1) along a streamline yields:

$$\left[\frac{1}{2}\rho v^2 + p\right]_{x_1}^{x_2} = \int_{x_1}^{x_2} (f_L)_x \, dx \qquad (B2)$$

where x is the coordinate along a streamline and $(f_L)_x$ the tangential component of $\vec{f_L}$. Equation (B2) is Bernoulli's equation with a force term added. Just below the electrode tip we have that $j_p << j_w$, so that the effect of j_p on $\vec{f_L}$ is negligible.

Now consider a streamline close to the drop surface, with x_1 well above, and x_2 just below the anode spot, and x_2 close to the axis – Fig. 8. This streamline enters the region where $j_w = 0$, at $x = x^*$, so that the main contribution to the integral in equation (B2) comes from the interval between x^* and x_2. As an approximation,

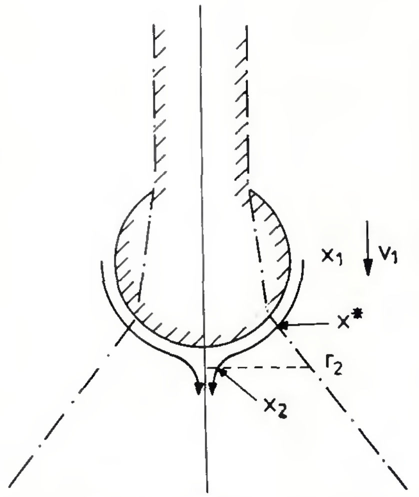

Fig. B – Diagram to illustrate discussion on pressure in the plasma. —.— indicates boundary where $j_W \neq 0$

we now replace the integral from x^* to x_2 by the integral in the radial direction from a point r_2 on the boundary of the region where $j_w \neq 0$, to the axis. Since $B_\theta \approx \mu_0 r j_w/2$, it follows from equations (B2) and (8) that:

$$p_0 - p_1 = \frac{1}{4}\mu_0 j_w^2 r_2^2 - \frac{1}{2}\rho(v_0^2 - v_1^2), \qquad (B3)$$

where p_0 and v_0 are the pressure and the flow velocity at the axis. It follows from equation (B3) that the upward force on the drop, in the absence of any gas flow, is given by:

$$\pi r_2^2 (p_0 - p_1) = \frac{\mu_0 I_w^2}{4\pi}.$$

The downward Lorentz force on the drop (equation (10)) will be compensated almost completely, because χ is of order unity. Typical values for the experiment discussed here are $v_1 = 50$ m/s, $I_w = 100$ A, $r_2 = 1$ mm, while $\rho \approx 0.07$ kg/m^3. It then follows that $p_0 - p_1 = 0$ when $v_0 \approx 100$ m/s. The difference $p_0 - p_1$ will certainly be positive, but this estimate shows that it is likely to be small.

C. Current Drawn by the Electrode

The lower half of the wire electrode is surrounded by a flowing plasma. The Reynolds number for the flow in the channel without the electrode is about 700, and the flow is assumed to be laminar. A thermal and a velocity boundary layer (Ref 35) will then be formed, both having a thickness of about 2 mm (0.08 in.). Furthermore, the electrode potential is, in general, not equal to the plasma potential; this leads to the formation of another boundary layer.

The latter consists (Ref. 31, 32, 41) of a thin (≈ 0.1 μm) space charge layer, where the ion density, n_+, is different from n_e. Outside this layer there is a region where $n_e \approx n_+$, and where the potential increases or decreases towards the plasma potential. The electron mean free path is about 2 μm, and the ion mean free path about 0.5 μm in the plasma discussed here; as a result the particles will not suffer collisions in the space charge sheath.

If the electrode is negative with respect to the plasma, then the density of the ion current to the electrode, j_+, is given by (Ref. 31):

$$j_+ = \frac{n_{+s}\bar{v}_+ e}{2} \qquad (C1)$$

and the density of the electron current, j_e, by:

$$j_e = \frac{n_{es}\bar{v}_e e}{2} \exp(e \Delta DV_s/k T_e) \qquad (C2)$$

where n_{+s} and n_{es} are the densities at the sheath edge, $\bar{v}_+$ and $\bar{v}_e$ the thermal velocities of ions and electrons, respectively, e the electron charge, ΔV_s the potential of the wire with respect to the potential at the sheath edge, T_e the electron temperature, and k Boltzmann's constant.

The velocities $\bar{v}_+$ and $\bar{v}_e$ are given by $\bar{v}_{+e} = (8 k T_{+e}/\pi m_{+e})^{1/2}$, where m_+ and m_e are the ion and the electron mass respectively, and T_+ is the ion temperature. The gas temperature, T_g, is equal to T_e in the unperturbed plasma, and both decrease in the direction of the electrode.

A recent analysis of the anode boundary layer of an argon arc by Dinulescu and Pfender (Ref. 41) showed that T_e decreases much more slowly than T_g. This is also expected to be so in the boundary layer around the electrode. The ion temperature will remain equal to T_g.

Experiments by Essers and Jelmorini (Ref. 28) in a plasma-GMA arc showed that the electrode draws an ion current at large negative potentials. The part of the electrode surrounded by the plasma was about 25 mm (1 in.) long in their experiment, the electrode diameter was 0.9 mm (0.04 in.), and the ion current 2 A independently of V_w at strongly negative voltages. It then follows that $j_+ \approx 3 \times 10^4$ A m^{-2}.

Inserting this value into equation (C1) with $T_+ = 1500$ K gives $n_{+s} = 4.1 \times 10^{20}$ m^{-3}. It is now assumed that n_{es} has the equilibrium value corresponding to T_e at the sheath edge. It follows from the Saha equation (Ref. 42) which relates n_e and T_e that:

$$\left(\frac{n_{es}}{n_{ep}}\right)^2 = \left(\frac{T_{es}}{T_{ep}}\right)^{3/2} \frac{T_{gp}}{T_{gs}} \exp \left\{ \frac{e\,E_i}{k\,T_{ep}} - \frac{e\,E_i}{k\,T_{es}} \right\} \qquad \text{(C3)}$$

where E_i is the ionization potential (15.8 V for Ar), and the subscripts p and s refer to values in the unperturbed plasma and at the sheath edge, respectively.

The above relation gives T_{es}, because $n_{es} \approx n_{+s}$, and n_{ep} and T_{ep} ($= T_{gp}$) are known ($n_{ep} = 1.4 \times 10^{23}$ m^{-3}, $T_{ep} = 13000$ K, Ref. 27). It is thus found that $T_{es} \approx 6800$ K. The relation between ΔV_s and the potential difference $\Delta V \equiv V_w - V_p$ has not, to our knowledge, been derived for cylindrical probes.

Results for spherical probes show that the drop in potential across the neutral part of the boundary layer is comparable in magnitude with ΔV_s. We, therefore, state as an approximation, that $\Delta V_s \approx \Delta V/2$. Equation (C2) then yields:

$$j_e = j_{es} \exp\,(e\,\Delta V/2\,k\,T_e) \qquad \text{(C4)}$$

where $j_{es} \equiv \dfrac{n_{es} \bar{v}_e\, e}{2} = 1.4 \times 10^7$ A m^{-2}.

Next, difference ΔV must be found. Equation (C2) also holds for the anode boundary layer. There is a metal vapor plasma in front of the anode spot, where $n_{ep} \approx 10^{22}$ m^{-3}, and $T_{ep} \approx 7000$ K (Ref. 27). The decrease in T_e has less effect than in the argon plasma, because E_i is lower (7.9 V for Fe, 7.4 V for Mn).

Comparing the arc discussed here with the arc investigated by Dinulescu and Pfender (Ref. 41), we expect T_{es} to lie between 4000 and 6000 K. Equation (C3) yields $n_{es} \approx 10^{21}$ m^{-3} for $T_{es} = 5000$ K, and it follows that $j_{es} \approx 4 \times 10^7$ A m^{-2}.

The current density at the drop surface is of comparable magnitude (100 A through several mm^2). It thus follows that ΔV_s will be slightly positive or negative, and the potential difference between the electrode tip and the adjacent plasma will be neglected.

The difference between n_e in the center of the arc and in the hotter outer zone leads to a potential difference between the two regions as shown below. There will be a diffusion of electrons and ions across the boundary from the hotter to the colder plasma, because of the difference in n_e. The current densities for electrons and ions must be equal in order to maintain a stationary state.

The diffusion coefficient for electrons is much larger than that for ions. Consequently, an electric field $\vec{E}_a$ is set up which accelerates ions and retards electrons. This process of ambipolar diffusion is described in several text books (Ref. 43) and is not here discussed in detail. It follows that:

$$\vec{E}_a = \frac{k\,T_e}{e} \frac{\vec{\nabla}\, n_e}{n_e} \qquad \text{(C5)}$$

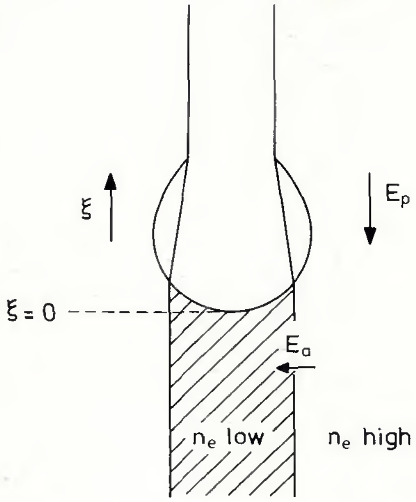

Fig. 9—Diagram to illustrate discussion on difference between electrode and plasma potential

Integration in the radial direction, across the boundary, gives the potential difference, ΔV_a, between the hotter ($n_e = n_{eh}$) and the colder ($n_e = n_{ec}$) plasma:

$$\Delta V_a = \frac{k\,T_e}{e} \ln \frac{n_{eh}}{n_{ec}}. \qquad \text{(C6)}$$

Taking an average value for T_e (10^4 K) we find, since $n_{eh}/n_{ec} \approx 10$, that $\Delta V_a \approx 2$ V.

The difference ΔV can now be given as a function of the vertical coordinate, ζ—Fig. 9. The argument given above shows that $V_w \approx V_p$ at $\zeta = 0$, and we take both V_p and V_w to be zero at $\zeta = 0$. We then have:

$$V_w = \frac{\rho_R\, I_w\, \zeta}{\pi\, R_w^2}$$

where ρ_R is the resistivity of the electrode material ($\rho_R \approx 1.3 \times 10^{-6} \Omega$ m). The plasma potential in the argon plasma is given by:

$$V_p = \Delta V_a + \zeta\, E_p$$

where E_p is the longitudinal electric field strength. It then follows that:

$$\Delta V \equiv V_w - V_p = -\Delta V_a - \zeta \left(E_p - \frac{\rho_R\, I_w}{\pi\, R_w^2} \right) \qquad \text{(C7)}$$

Insertion of the data given above, with $I_w = 200$ A yields:

$$\Delta V = -2 - \zeta\,(10^3 - 0.13 \times 10^3)$$

where ΔV is in V, and ζ in m.

It is seen that ΔV is negative, and that its absolute value increases with increases in ζ. The electron current which enters the electrode above the coordinate is given by:

$$I_e(\zeta) \equiv 2\,\pi\, R_w \int_\zeta^\infty j_e(\zeta')\, d\infty'.$$

Substitution of equations (C4) and (C7) with j_{es} as given above yields:

$$I_e(\zeta) \approx 15 \exp\,(-700\,\zeta)$$

when I_e is in A, and ζ in m.

It is to be noted that this expression only holds for the electrode surface which is in contact with the hotter argon plasma. It does not hold down to $\zeta = 0$, because the lower surface of the electrode tip is in contact with the metal plasma. The values of I_e for $\zeta = 1$ and 2 mm (0.04 and 0.08 in.) are 7 and 4 A, respectively.

The drop length is at least 1 mm (0.04 in.) in all the experiments. Consequently, an electron current of 5 to 10 A will enter the electrode above the drop if the drop is small, i.e., if I_w is high. The electrode potential in the electrode's upper part is well below V_p. Electron emission will, however, not occur, because the electrode is too cold. An ion current of about 4 A will be drawn and will partly compensate the electron current.

In summary, the current passing through the drop might be different from the electrode current by about 10 A when I_w is high (150–200 A).

D. List of Symbols Used in More Than One Section

$\vec{B}$	magnetic induction
d_w	electrode diameter
C_d	drag coefficient for drop
C_{ds}	drag coefficient for sphere
F_d	drag force
F_{em}	electromagnetic force
$\vec{F}_L$	Lorentz force
$\vec{f}_L$	Lorentz force per unit volume
$\vec{j}$	current density
I_p	plasma current
I_w	wire current
M	drop mass
n_e	electron number density
R	drop radius
Re	Reynolds number
R_w	wire radius
S	cross-sectional area of channel
T	temperature
T_e	electron temperature
T_{eff}	effective gas temperature
T_0	room temperature
$\dot{V}$	gas flow rate
v	velocity
z	axial coordinate
α	angle (Fig. 6)
β	angle (Fig. 6)
γ	surface tension
η	viscosity
μ_0	permeability of vacuum
ρ	mass density
χ	form factor (equation (11))